*Second International Conference on Motion and Vibration Control, Yokohama, Aug.30 - Sept.3, 1994*

# Active Control of a Silicon-Wafer Slicer Cutting a Crystal Ingot (Effect on the Deflection Control of the Air Film Stiffness between the Blade and the Ingot)

***Keijiro Masui*, Seiji Chonan ** and Zhong-Wei Jiang*****

** Graduate School, Tohoku University, Sendai, Miyagi 980, Japan*
*** Department of Aeronautics and Space Engineering, Tohoku University, Sendai, Miyagi 980, Japan*

## Abstract

Response of an ID sawblade slicing a crystal ingot is studied analytically with the effect of the air film stiffness between the ingot and the blade taken into account. The rotating blade is clamped and stressed initially in the radial direction along the outer periphery, while the inner edge is subjected to both the stationary in-plane and the dynamic lateral slicing load from the workpiece. The solution is obtained by introducing the Fourier expansion method, further applying the Galerkin method to the governing equations of the system. The distributed air film between the blade and the ingot is approximated by a set of parallel translational springs. Numerical results are presented for an actual SUS301 blade cutting a 6″-diameter silicon ingot at a speed of 1550 rpm. Effects on the blade deflection of the stiffness and location of the springs are examined numerically. Results obtained show that the blade deflection is much affected by the air film stiffness, further the flatness of the rotating blade is improved by controlling the air flow rate and increasing appropriately the air film stiffness between the blade and the ingot.

## 1. Introduction

The ID (inner-diameter) saw blade is nowadays commonly used in the crystal wafering. Demands on large-diameter silicon wafer have accelerated the development of the large-scale ingot slicer. Further, high performance of the IC devices has made it a necessity to provide silicon wafers with adequately flat, parallel sides. To meet these requirements both for the slicer and for the wafer, it appears that the introduction of active control is indispensable to the development of a highly efficient slicer.

Several papers have been published in recent years on the vibration and control of rotating disks. Ellis et al. [1] analyzed a feedback vibration controller that increases the transverse stiffness and damping of a circular OD (outer-diameter) saw. Radcliffe et al. [2] used an on-line FFT analysis of the rotating disk displacement to suppress the amplitude of the dominant mode. Hutton et al. [3] analyzed the response of OD sawblade with stationary point springs. Huang et al. [4] investigated a circular line guide system to increase the critical speed of a spinning annular plate. Chonan et al. [5] obtained the in-plane stress distribution in a silicon-wafer slicer cutting a crystal ingot taking into account all stresses from the spinning, the initial tensioning in the radial direction and the in-plane reaction from the workpiece. They further studied the natural vibration of the rotating ID saw with the in-plane stresses and obtained the deflection of the blade subjected to the static lateral cutting force [6].

During the crystal wafering by the ID sawblade, the air film is formed between the blade and the ingot. It appears, to the authors' knowl-

edge, that the characteristics of the ID sawblade slicing a crystal ingot have not been studied appropriately with the effect of the air film stiffness taken into account. Chonan et al. [7] showed that the air film stiffness is controlled by regulating the air flow rate supplied to the air film.

In this paper, the response of an ID sawblade slicing a crystal ingot is studied analytically with the effect of the air film stiffness between the ingot and the blade taken into account. Numerical results are presented for an actual SUS301 blade cutting a 6″-diameter silicon ingot at a speed of 1550 rpm. The distributed air film between the blade and the ingot is approximated by a set of parallel translational springs. Effects on the blade deflection of the spring stiffness and the location are studied in detail.

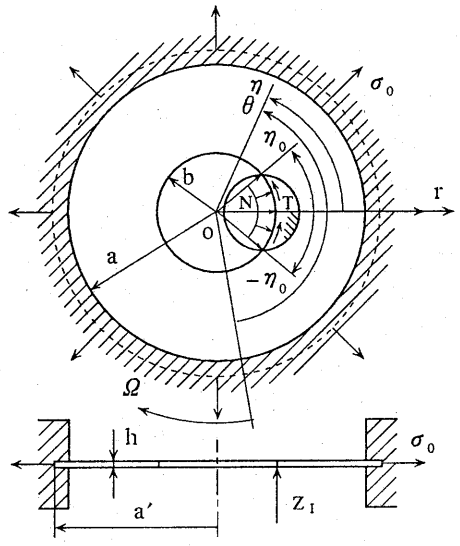


Fig. 1 Geometry of problem and coordinates.

## 2. Formulation and Analysis

### 2.1 Governing Equations

Figure 1 shows an ID saw blade slicing a silicon ingot at a constant angular speed $\Omega$. The blade has a thickness $h$ and is free at the inner edge ($r = b$). After initially tensioned in the radial direction by the radial stress $\sigma_0$ along the outer periphery $r = a'$, the blade is clamped from both sides by two rigid rings on the range $a \leq r \leq a'$. In the figure, the system $(r,\theta)$ is a co-ordinate frame rotating with the blade, while the $(r,\eta)$ another frame fixed in space. The cutting force is decomposed into in-plane radial compressive force $N$ (Pa), circumferential shear force $T$ (Pa) and axial lateral force $Z_I$ (N). Each of them is assumed uniformly distributed over the arc $| \eta | \leq \eta_0$ along the inner periphery of blade. The lateral cutting force $g(r,\eta,t)$ acting on the blade is generally represented by

$$g(r,\eta,t) = \sum_{k=1}^{K} q_k(t)(1/r)\delta(r - r_k)\delta(\eta - \eta_k), \qquad (1)$$

where $\delta(\ )$ is the Dirac delta function and $K$ is the total number of concentrated lateral forces assumed. The problem discussed in the following is the effect on the blade deflection of the air film stiffness between the blade and the ingot. The distributed air film is approximated by a set of parallel translational springs. Denoting the stiffness of the equivalent springs by $k_s$, the air film reaction to the deflection of blade is written in the form

$$s(r,\eta,t) = \sum_{k=1}^{K_c} k_s w_k(1/r)\delta(r - r_k)\delta(\eta - \eta_k), \qquad (2)$$

where $K_c$ is the number of the equivalent springs assumed.

The equation governing the flexural vibration of the blade referred to the co-ordinate frame fixed in space is

$$\begin{aligned} &D[\partial^2/\partial r^2 + (1/r)\partial/\partial r + (1/r)^2\partial^2/\partial\eta^2]^2 w \\ &\quad +\rho h[\partial/\partial t - \Omega\partial/\partial\eta]^2 w \\ &\quad -h[(1/r)\partial/\partial r(r\sigma_r\partial w/\partial r) \\ &\quad +(1/r^2)\partial/\partial\eta(\sigma_\eta\partial w/\partial\eta) \\ &\quad +(1/r)\partial/\partial r(\tau_{r\eta}\partial w/\partial\eta) \\ &\quad +(1/r)\partial/\partial\eta(\tau_{r\eta}\partial w/\partial r)] \\ &\quad = g(r,\eta,t) - s(r,\eta,t), \end{aligned} \qquad (3)$$

where $w(r,\eta,t)$ is the lateral displacement of the blade, $D(= Eh^3/12(1-\nu^2))$ is the flexural rigidity, $E$ is the Young's modulus, $\nu$ is the Poisson's ratio and $\rho$ is the mass density of blade; $\sigma_r$ is the in-plane radial normal stress, $\sigma_\eta$ the hoop stress, and $\tau_{r\eta}$ the shear stress in the rotating blade, which are presented in Reference [5].

One assumes the solution of equation (3) in the Fourier series as

$$\begin{aligned} w(r,\eta,t) = \sum_{m=0}^{M}\sum_{n=0}^{N} &[C_{mn}(t)\cos(n\eta) \\ &+S_{mn}(t)\sin(n\eta)]R_{mn}(r). \end{aligned} \qquad (4)$$

Here, $R_{mn}$ is the mode function of a non-rotating stationary blade clamped along the outer boundary ($r = a$) while free at the inner edge ($r = b$); $m$

and $n$ are the numbers of nodal circles and diameters on the blade. $R_{mn}$ is given by

$$R_{mn}(r) = \mathrm{J}_n(k_{mn}r) + F_{mn}\mathrm{Y}_n(k_{mn}r) + G_{mn}\mathrm{I}_n(k_{mn}r) + H_{mn}\mathrm{K}_n(k_{mn}r), \quad (5)$$

where $\mathrm{J}_n$ and $\mathrm{Y}_n$ are the Bessel functions of the first and second kinds, and $\mathrm{I}_n$ and $\mathrm{K}_n$ are the modified Bessel functions; $F_{mn}$ through $H_{mn}$ and $k_{mn}$'s are the unknowns and eigenvalues determined from the boundary conditions of the blade.

Substituting equation (4) into equation (3), further applying the Galerkin method to the resulting equation, one has a system of simultaneous ordinary differential equations of the form

$$\boldsymbol{M}\ddot{\boldsymbol{X}} + \boldsymbol{\Gamma}\dot{\boldsymbol{X}} + \boldsymbol{K}\boldsymbol{X} = \boldsymbol{Q}q_k(t), \quad (6)$$

where

$$\boldsymbol{X} = [C_{00}(t), \cdots, C_{M0}(t), C_{01}(t), S_{01}(t), \cdots, C_{MN}(t), S_{MN}(t)]^{\mathrm{T}}. \quad (7)$$

Here, $\boldsymbol{M}$, $\boldsymbol{\Gamma}$, and $\boldsymbol{K}$ are matrices of the dimension $[(p+1)(2q+1)] \times [(p+1)(2q+1)]$; $\boldsymbol{K}$ is the stiffness matrix on the air film stiffness $k_s$; $\boldsymbol{Q}$ is the column vector showing the locations of the lateral cutting force, which is given by equation (1).

### 2.2 Steady-State Deflection of Rotating Blade Subjected to Lateral Cutting Force

An assumption is made that the blade is deformed laterally by the reaction force $Z_I(\eta_0)$ from the ingot. The $Z_I$ is approximated by a set of concentrated forces that are distributed uniformly over the arc $|\eta| \leq \eta_0$ along the inner periphery of blade ($r = b$). Thus $q_k$ and $r_k$ in the equation (1) are given as

$$q_k = Z_I/K, \; r_k = b. \quad (8)$$

Here, $Z_I$ is the magnitude of total axial cutting force, and $K$ is the number of concentrated forces assumed.

It is assumed that the system has been reached to a steady state. In this case, the time invariant solution of the blade is obtained from

$$\boldsymbol{K}\boldsymbol{X} = \boldsymbol{Q}q_k. \quad (9)$$

After having $X$ from the above equation, the steady deflection $w(r, \eta)$ of the rotating blade is calculated by substituting $C_{mn}$ and $S_{mn}$ into equation (4).

### 2.3 Vibration of Blade Subjected to Lateral Disturbance

The blade cutting an ingot is subjected to various disturbances that are attributed to the inhomogeneous diamond abrasive grit or the vibration of spindle. In this section, a half-sine shock pulse is assumed as a disturbance that excites the blade. Denoting the intensity of the disturbance by $A$, and the angular frequency by $\omega_0$, one has $q_k$ in equation (1) as

$$q_k(t) = \begin{cases} (A/K)\sin\omega_0 t & (0 \leq t \leq \tau) \\ 0 & (\tau < t), \end{cases} \quad (10)$$

where $\tau(= \pi/\omega_0)$ is the time of duration of the disturbance.

Equation (6) is rearranged in the state equation as

$$\dot{\boldsymbol{x}}(t) = \boldsymbol{A}\boldsymbol{x}(t) + \boldsymbol{B}q_k(t), \quad (11)$$

where

$$\boldsymbol{x} = \begin{bmatrix} \boldsymbol{X} \\ \dot{\boldsymbol{X}} \end{bmatrix}, \quad (12)$$

$$\boldsymbol{A} = \begin{bmatrix} \mathbf{o} & \boldsymbol{I} \\ -\boldsymbol{M}^{-1}\boldsymbol{K} & -\boldsymbol{M}^{-1}\boldsymbol{\Gamma} \end{bmatrix}, \quad (13)$$

$$\boldsymbol{B} = \begin{bmatrix} \mathbf{o} \\ -\boldsymbol{M}^{-1}\boldsymbol{Q} \end{bmatrix}. \quad (14)$$

The natural frequencies of the blade are obtained from

$$|\boldsymbol{A} - \omega\boldsymbol{I}| = 0. \quad (15)$$

The imaginary part of the eigen value $\omega$ corresponds to the natural angular frequency of the rotating blade. The displacement of the blade is obtained from the equation.

$$w(r, \eta, t) = \boldsymbol{C}\boldsymbol{x}(t), \quad (16)$$

where

$$\boldsymbol{C} = [R_{00}(r), \cdots, R_{M0}(r), \cos(\eta)R_{01}(r), \sin(\eta)R_{01}(r), \cdots, \cos(N\eta)R_{MN}(r), \sin(N\eta)R_{MN}(r), 0 \cdots 0]. \quad (17)$$

## 3. Numerical Results and Discussions

Numerical results that follow are for a SUS 301 blade cutting a 15.24cm (6″) diameter silicon ingot. The physical parameters of the blade measured are given in Table 1. Here,

Table 1 Physical parameters of slicing blade.

| | | | |
|---|---|---|---|
| $a'$ | 0.3125 m | $\nu$ | 0.28 |
| $a$ | 0.298 m | $\rho$ | $7.84\times10^{3}$ kg/m$^3$ |
| $b$ | 0.120 m | $E$ | $1.99\times10^{11}$ N/m$^2$ |
| $h$ | $0.15\times10^{-3}$ m | $\sigma_0$ | $7.05\times10^{8}$ N/m$^2$ |

$\sigma_0$ is the initial radial tension at the outer periphery ($r = a'$) that was applied to the blade so that the inner hole of the blade is increased by $\Delta b$ = 1mm.

In the following analysis, the results are obtained for the maximum contact angle between the blade and the ingot. The contact angle $\eta_0$ is calculated analytically from the next equation as a function of the cutting depth of ingot $x_I$:

$$\eta_0(x_I) = \cos^{-1}\left[1 - \frac{x_I(2a_I - x_I)}{2b(x_I - a_I + b)}\right], \qquad (18)$$

where $a_I$ is the radius of ingot. The maximum contact angle between the blade and the ingot is calculated as $\eta_{0MAX} = 39.42°$, while the maximum lateral reaction at this contact angle was measured $Z_I = 4.02$ N for the sawblade cutting the 6″diameter ingot. As mentioned above, the lateral load is approximated by a set of concentrated forces that are distributed uniformly over the arc $|\ \eta\ | \leq \eta_{0MAX}$. In the calculation that follows, the number of concentrated forces was assumed $K = 100$. The series terms of equation (4) were considered up to $M = 1$ and $N = 4$.

Figure 2 shows the working ID sawblade slicing the ingot. As presented in the figure, the air film is formed between the blade and the ingot. The distributed air film stiffness between the blade and the ingot is approximated by a set of parallel translational spring stiffness. In the next section, the behaviour of the blade slicing the ingot will be studied numerically with the effect of the air film stiffness taken into consideration.

### 3.1 Effect of Air Film Stiffness and Distribution on the Deflection of Blade

Variation of inner edge deflection with an increase of the air film stiffness is examined first. As shown in Fig. 3, the air film stiffness on the contact area is approximated by 19 concentrated spring stiffness ( $K_c = 19$ ) for the maximum contact angle $\eta_{0MAX} = 39.42°$. The symbol "×" in the figure shows the location of the springs introduced. Figure 4 shows the blade deflection along the inner edge ($r = b$) for several values of the air film stiffness $k_s$. It is observed that the deflection of the edge is significantly reduced with an increase of the air film stiffness.

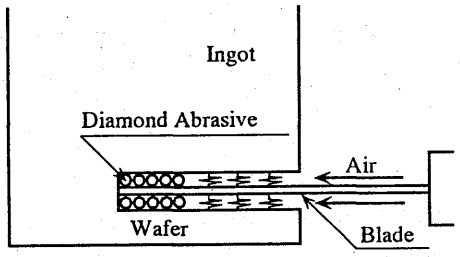


Fig. 2 Blade cutting the ingot.

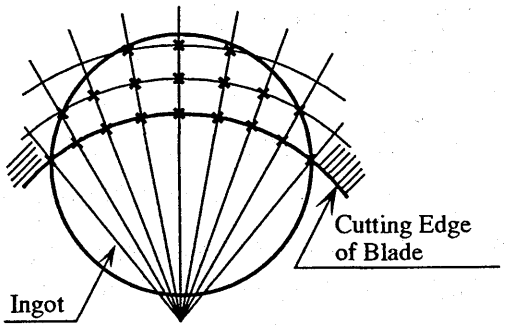


Fig. 3 Air film stiffness approximated by distributed spring stiffness.

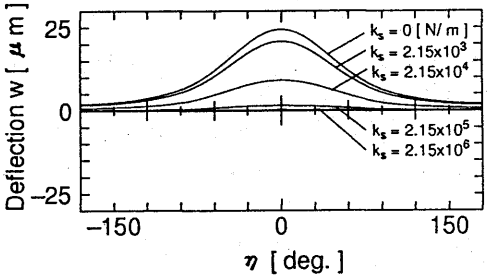


Fig. 4 Variation of inner edge deflection with an increase of the air film stiffness.

It is said in general that the air pressure is not distributed uniformly in the contact area. The effect of the distribution of air film stiffness is studied next. The spring stiffness $k_s$ multiplied by the number of springs $K_c$ is assumed constant ( $k_s K_c = 40.8 \times 10^6$ N/m ) and the locations of the springs are changed.

The case of the air film springs distributed uniformly along the diameter that is located at the center of contact area is studied first. Figure 5 shows the air film springs located at three points on the diameter $\eta = 0°$. The spring stiffness is

constant and given by $k_s = 13.6 \times 10^6$ N/m. Figure 6 shows the deflection of the inner edge for the spring locations of Fig. 5. It is observed that the deflection at $\eta = 0°$ is reduced by the stiffness of the air film. In this case, the suppression of the total deflection along the cutting edge cannot be realized even if the air film stiffness is increased. This comes from the fact that the circumferential width of distribution of the springs is not enough.

Next, the air film stiffness is assumed uniformly distributed on the same circle ($r = b$) as given in Fig. 7. Figure 7(a) shows the case where the springs are located along the whole contact area ($|\eta| \leq \eta_{0MAX}$, $k_s = 4.54 \times 10^6$ N/m, $K_c = 9$ ), while (b) the case of the springs distributed partially on $|\eta| \leq 20°$ ( $k_s = 8.16 \times 10^6$ N/m, $K_c = 5$ ). Figure 8 shows the deflection along the inner edge for the two cases of distribution. When the width of distribution is not enough, the reduction of deflection is not remarkable, while it is satisfactory for the case of the wide distribution, as can be seen from Fig. 8(a).

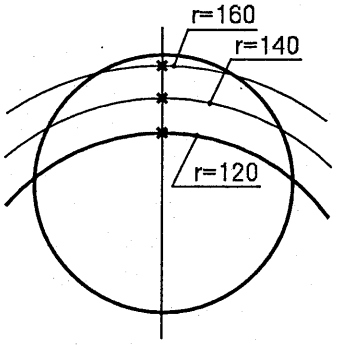


Fig. 5 Air film stiffness distributed along the diameter located at the center of contact area. $k_s = 13.6 \times 10^6$ N/m, $K_c = 3$.

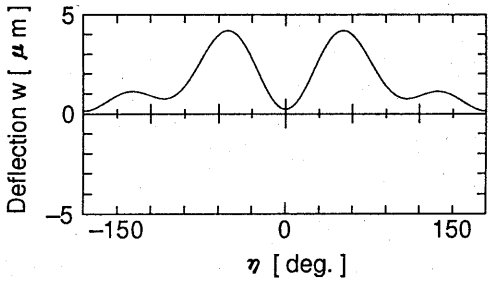


Fig. 6 Deflection of inner edge for air stiffness distribution of Fig. 5.

As mentioned above, the air film stiffness can be increased or decreased actively by controlling the air flow rate between the blade and the ingot. The results obtained above show that the air should be supplied to the optimum direction so that the air film stiffness is increased uniformly in the circumferential direction.

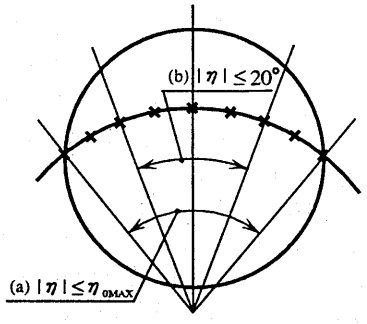


Fig. 7 Air film stiffness distributed on the same circle ($r = b$). (a) $|\eta| \leq \eta_{0MAX}$, $k_s = 4.54 \times 10^6$ N/m, $K_c = 9$; (b) $|\eta| \leq 20°$, $k_s = 8.16 \times 10^6$ N/m, $K_c = 5$.

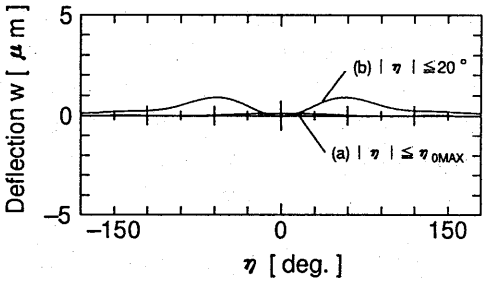


Fig. 8 Deflection of inner edge for air stiffness distribution of Figs. 7(a) and (b).

### 3.2 Shock Response of Blade Subjected to Lateral Disturbance

The shock response of the blade subjected to the dynamic disturbance is studied in this section. Figure 9 shows the variations of natural frequencies of the blade with an increase of the rotation speed. In the figure, the dotted line shows the case of no air film stiffness, while the solid line the case of the blade with a set of air film springs. The springs are placed at the locations "×" shown in Fig. 3. The spring stiffness is $k_s = 2.15 \times 10^6$ N/m. The critical speed (the speed at which stationary constant force will produce resonance) of the blade with air springs is not much affected by the air film stiffness. However, the modal coupling is observed and the frequencies are increased compared with the case of $k_s = 0$.

The transient response of the blade is studied next. A half-sine shock pulse is applied to the blade. The total force of the disturbance is 4.02N, which is assumed uniformly distributed along the inner periphery ($r = b$) over the arc $|\eta| \leq \eta_0$. The

contact angle $\eta_0$ is assumed maximum and given by $\eta_{0MAX} = 39.42°$. The blade is subjected to the lateral disturbance at the maximum contact angle, further the angle $\eta_0$ is assumed constant during the transient response of blade, i.e., $\eta_0 \simeq \eta_{0MAX}$. The displacement of blade is observed at the center of the inner edge ($r = b$, $\eta = 0°$) for several values of the input duration. Figure 10 shows the variations of the peak displacement with an increase of the input duration $\tau$ taking the air film stiffness $k_s$ as a parameter. For the blade without the air film stiffness ($k_s = 0$), the natural frequency of the fundamental $(0,0)$ mode is 458 Hz and the half period is $\tau_{00} = 1.09$msec when the rotation speed of blade is 1550 rpm. In this case, the peak displacement takes on maximum when $\tau/\tau_{00}$ =0.8 or 2. When $\tau/\tau_{00}$ =0.8, both the $(0,0)$ and $(0,1)$ modes are the dominant modes. On the other hand when $\tau/\tau_{00} = 2$, just the $(0,0)$ mode is dominant. For the case of the blade with the air springs located at the positions "×" of Fig. 3, the peak displacement is reduced over the whole frequency, which was found to become more significant with an increase of the air film stiffness.

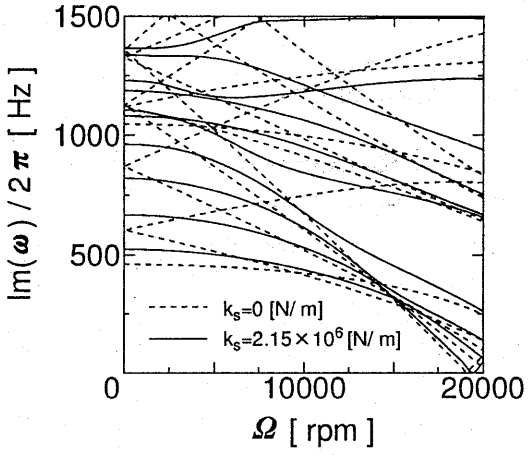


Fig. 9 Variation of natural frequencies of blade with an increase of rotation speed.

## 4. Conclusions

A theoretical analysis has been presented for the response of the rotating blade of wafer slicer subjected to the slicing load from the workpiece. The effect on the blade deflection of the air film stiffness between the ingot and the blade has been studied in detail. The results obtained show that the blade deflection is much affected by the air film stiffness, further the flatness of the blade is improved by controlling the air flow rate and increasing the air film stiffness appropriately between the blade and the ingot. It is concluded that the air should be supplied to the direction that increases the air film stiffness uniformly in the circumferential direction.

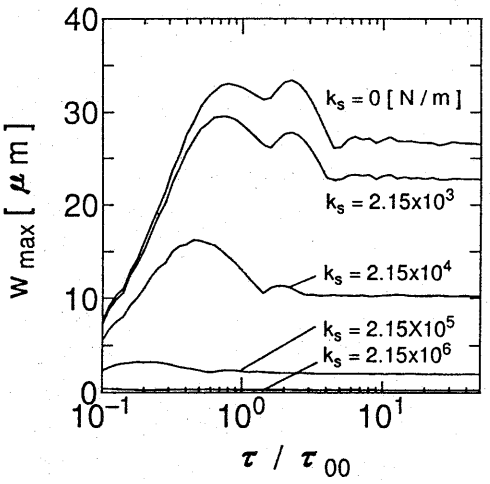


Fig. 10 Maximum displacement of blade at the center of inner edge versus pulse duration.

## References


[1] Ellis, R. W. and Mote, C. D., Jr., A Feedback Vibration Controller for Circular Saws,ASME J. Dyn. Sys., Meas., Cont., 101, (1979), 44.

[2] Radcliffe,C.J. and Mote,C.D.,Jr., Identification and Control of Rotating Disk Vibration, ASME J. Dyn. Sys., Meas., Cont., 105, (1983), 39.

[3] Hutton,S.G., Chonan,S. and Lehmann,B.F., Dynamic Response of a Guided Circular Saw, J. Sound and Vib., 112–3, (1987), 527.

[4] Huang,S.C. and Hsu.B.S, Vibrations of a Spinning Annular Plate with Multi-Circular Line Guides, J. Sound and Vib., 164–3, (1993), 535.

[5] Chonan,S., Jiang,Z.W. and Yuki,Y., Stress Analysis of a Silicon-Wafer Slicer Cutting the Crystal Ingot, ASME J. Mech. Desi., 115, (1993), 711.

[6] Chonan,S., Jiang,Z.W. and Yuki,Y., Vibration and Deflection of a Silicon-Wafer Slicer Cutting the Crystal Ingot, ASME J. Vib. Acous., 115, (1993), 529.

[7] Chonan,S., Jiang,Z.W. and Shyu,Y.J., Stability Analysis of a 2″Floppy Disk Drive System and the Optimum Design of the Disk Stabilizer, ASME J. Vib. Acous., 114, (1992), 283.